Elastic full-waveform inversion: Enhance imaging for legacy and modern acquisition

Faqi Liu[1], Cosmin Macesanu[1], Hao Xing[1], Matvey Romanenko[2], Ge Zhan[1], Carlos Calderón-Macías[1], and Bin Wang[1]

https://doi.org/10.1190/tle44050338.1

Abstract

Full-waveform inversion (FWI) has become the key algorithm in seismic processing workflows to derive high-resolution velocity models. Benefiting from accurate wavefield propagation in geologically complex areas, elastic FWI is able to produce superior velocity models with greatly improved resolution when compared to acoustic algorithms. In this paper, we apply FWI (both acoustic and elastic) to data acquired using different survey geometries including sparse-node data, legacy narrow-azimuth data, and distributed acoustic sensing-vertical seismic profile survey data to demonstrate the advantages. The increased physics in elastic FWI allows for significantly improved focusing of velocity interfaces with strong contrast, resulting in improved imaging of underneath structures.

Introduction

Full-waveform inversion (FWI) has been developed as the core of a seismic processing workflow to derive accurate velocity models with high resolution, from which a synthetic data set can best match the recorded one (Routh et al., 2017). FWI algorithms are largely differentiated with the different definition of "best match" represented in the objective functions. The derived models from FWI are typically used for depth migration. On the other hand, high-frequency FWI models have also been used to directly derive a reflectivity model commonly referred to as FWI image (Wang et al., 2021a) or FWI-derived reflectivity (Kumar and Ali, 2024). This high-resolution reflectivity is theoretically equivalent to an image from a nonlinear version of least-squares reverse time migration (RTM) (Wang et al., 2021a).

Due to the elastic nature of the earth, elastic FWI (EFWI) has intrinsic advantages over the acoustic version, especially in geologically complex areas like those with massive salt bodies (Raknes et al., 2015; Wang et al., 2021b; Liu et al., 2024). The elastic wave equations can simulate both compressional (P waves) and shear waves (S waves), capturing more detailed information about the subsurface. Even though EFWI has mainly been focusing on inverting V_P here, incorporating elastic effects in the inversion flow can result in more accurate P-wave propagation. These elastic effects come from the coupling of pressure waves with shear waves in the presence of strong gradient of shear velocity and density (ρ), which often occur at the interfaces with strong contrast of medium properties. Acoustic FWI (AFWI), in contrast, ignores the S-wave component and only accounts for the impacts of V_P and ρ, making it less effective in high-contrast media like the boundary of salt or basalt bodies. This can lead to less optimal imaging for complex underneath structures, such as faults and fractures, and inferior inversion results for reservoir properties.

Figure 1 shows a comparison of a snapshot and a simulated shot gather of the pressure data in an acoustic and elastic medium, respectively. Figures 1a and 1b show the P-wave snapshot overlaid on the P-wave velocity (V_P). The source is injected into the pressure component to simulate a marine case. As indicated by the yellow arrows, the salt boundary makes the elastic wavefield different from that of the acoustic data. A clear phase rotation is observed in the elastic shot gather (Figure 1d) comparing to Figure 1c. In addition, the red arrow in Figure 1b points to an event that is completely missing in the acoustic wave snapshot in Figure 1a. This is an event through double mode conversion at the salt boundary: a P wave converts to S wave entering the salt body, which is converted back to P wave while exiting the salt. Such an event is also observed in the shot gather in Figure 1d.

The incorporation of S-wave effects makes EFWI more accurate and robust when a medium presents large contrasts. By employing a more accurate simulation of the wavefields, EFWI

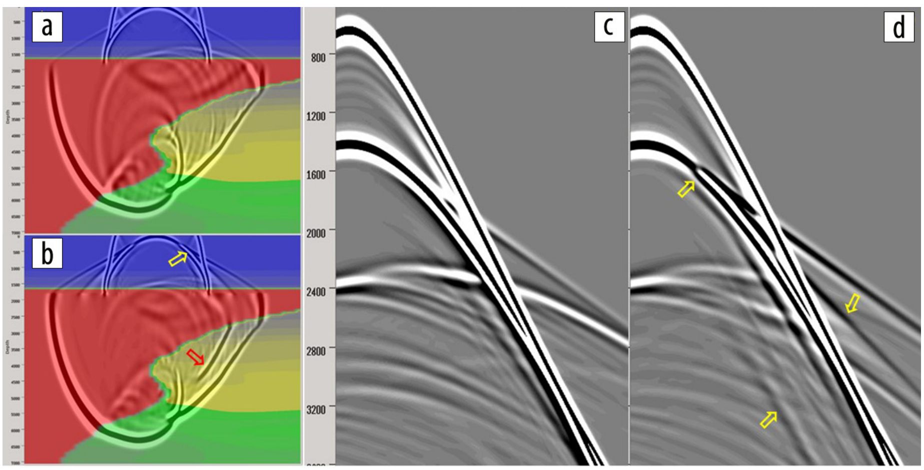

Figure 1. A snapshot for (a) acoustic and (b) elastic wave propagation. One synthetic shot gather of (c) acoustic and (d) elastic simulation. The red arrow points to a double mode-converted wave from P to S and back to P in (b).

Manuscript received 8 January 2025; accepted 10 February 2025.
[1]TGS, Houston, Texas, USA. E-mail: faqi.liu@tgs.com; cosmin.macesanu@tgs.com; hao.xing@tgs.com; ge.zhan@tgs.com; carlos.calderon@tgs.com; bin.wan@tgs.com.
[2]TGS, London, England. E-mail: matvey.romanenko@tgs.com.

results in more focused interfaces with strong contrast, like a salt boundary with a reduced salt halo, which often produces improved imaging quality below salt (Plessix and Krupovnickas, 2021). Additionally, elastic wave propagation can accurately simulate the mode-converted wave at strong interfaces as pointed to by the arrows in Figures 1b and 1d. Proper imaging of such events can significantly improve the image beneath the salt, where typically weak illumination is experienced with pure P-wave signal only. This may be particularly important for certain acquisition geometries like distributed acoustic sensing-vertical seismic profile (DAS-VSP) acquisition and multicomponent data. However, this improvement relies on a relatively accurate V_S and ρ model, either obtained a priori through realistic V_P/V_S and ρ relations estimated from additional information like well data, or they can be inverted jointly or in a staged approach.

In this paper, we demonstrate in different cases that EFWI has clear advantages over AFWI by using data sets collected from geologically complex areas (deepwater Gulf of Mexico [GoM] and the Nile Delta region). In the first case, elastic dynamic-matching FWI (DM FWI) is applied to a sparse ocean-bottom node (OBN) data set using, as input, the raw hydrophone component with limited preprocessing (Mao et al., 2020). Sparse OBN acquisition is currently the most cost-effective solution for deriving high-resolution velocity models, taking advantage of the long- to super-long offsets, full azimuth, and high signal-to-noise ratio (Huang et al., 2020). The EFWI presented here, utilizing the elastic wave equations for wavefield propagation, focuses on inverting V_P, whereas the other elastic parameters (V_S and ρ) are updated passively following empirical relations derived from well constraints. The impact of EFWI in areas with high-impedance contrasts is also demonstrated by its application to narrow-azimuth data from the Nile Delta region. In addition, we apply EFWI to a DAS-VSP data set from the GoM to demonstrate its effectiveness compared to AFWI. In this example, properly simulated mode-converted PS waves with elastic propagation help produce higher-quality images than in the acoustic case.

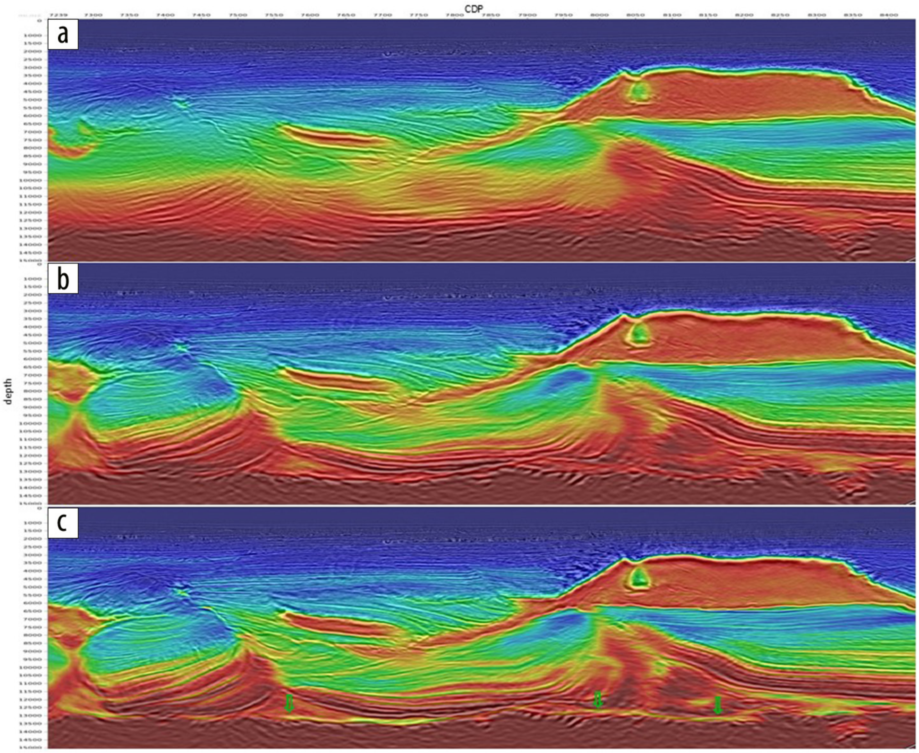

Figure 2. TTI RTM image of WAZ data using (a) FWI initial velocity model, (b) acoustic DM FWI model, and (c) elastic DM FWI model. Note, both AFWI and EFWI were applied to the sparse-node OBN data.

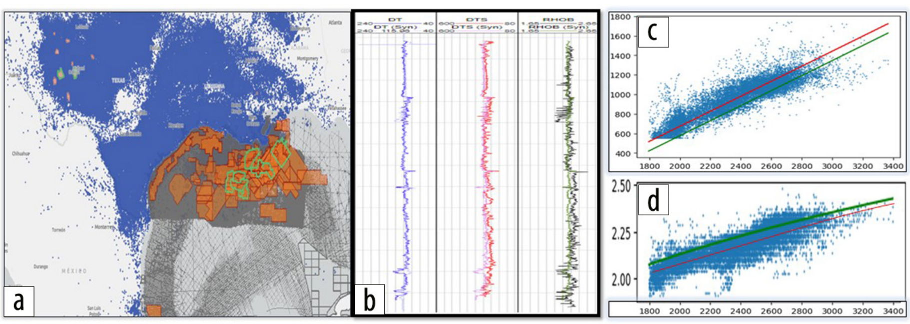

Figure 3. An areal map showing the area of the available well data. (b) One of the wells showing sonic, shear, and density logs. Matched relation between (c) V_S and (d) density with P-wave velocity for the well in (b). The red line is the matched relations for the current well, and the green line is the average of multiple wells in the area.

Sparse-node data from the GoM

Elastic DM FWI was applied to sparse-node data acquired in the GoM, where the massive complex salt bodies bring significant challenges to build a velocity model with high fidelity. The data were acquired with a maximum offset of 45 km. Multicomponent receivers were sparsely placed on the ocean floor with 1.2 km separation in both horizontal directions. Two source vessels with triple sources each were combined to allow for the recording of low-frequency signal below 2 Hz.

Starting with a legacy velocity model, both acoustic DM FWI and the elastic extension are applied to hydrophone data after limited preprocessing including deblending, debubble, and basic denoise. For QC purposes, a wide-azimuth (WAZ) data set is used as input to RTM using each of the velocity models before and after the inversions. The resulting images overlaying the corresponding velocity models are shown in Figures 2a–2c, respectively. In this application, elastic DM FWI was applied to invert V_P up to 18 Hz. Reliable relations of V_S and ρ with V_P derived from well data are shown in Figure 3. Comparing to the initial model and the corresponding RTM image in Figure 2a, acoustic DM FWI significantly improves the salt geometry. Notice also from the corresponding RTM image in Figure 2b the improved signal continuity below salt.

Elastic DM FWI improves the accuracy of the velocity model, as demonstrated by better focusing of the salt boundaries known as reduced salt halos and improved image resolution beneath the salt. Improvements in the salt definition also result in a better image at the Luan salt level, as observed in the RTM image of Figure 2c (pointed to by green arrows).

For a closer comparison between the AFWI and EFWI results, a zoomed version is shown in Figure 4. In the figure, the elastic wave propagation produces much better focused salt boundaries at both top and base of salt, described by a more compact interface and reduced halo than in the acoustic case, as shown by the green arrows in Figure 4b. The improved construction of the salt body results in enhanced focusing beneath it, especially the identification of a thin low-velocity layer pointed to by the red arrows. Figures 4c and 4d compare the FWI images derived from these models. Figures 4e and 4f show a depth slice for the AFWI- and EFWI-derived images. The EFWI model produces a much improved image with high resolution, in particular, the faults below the salt are clearly reconstructed in Figure 4d (pointed to by the two yellow arrows). They are not clearly noticeable in the acoustic result in Figure 4c. In addition, the depth slice displays significant improvement in lateral resolution of EFWI versus AFWI images.

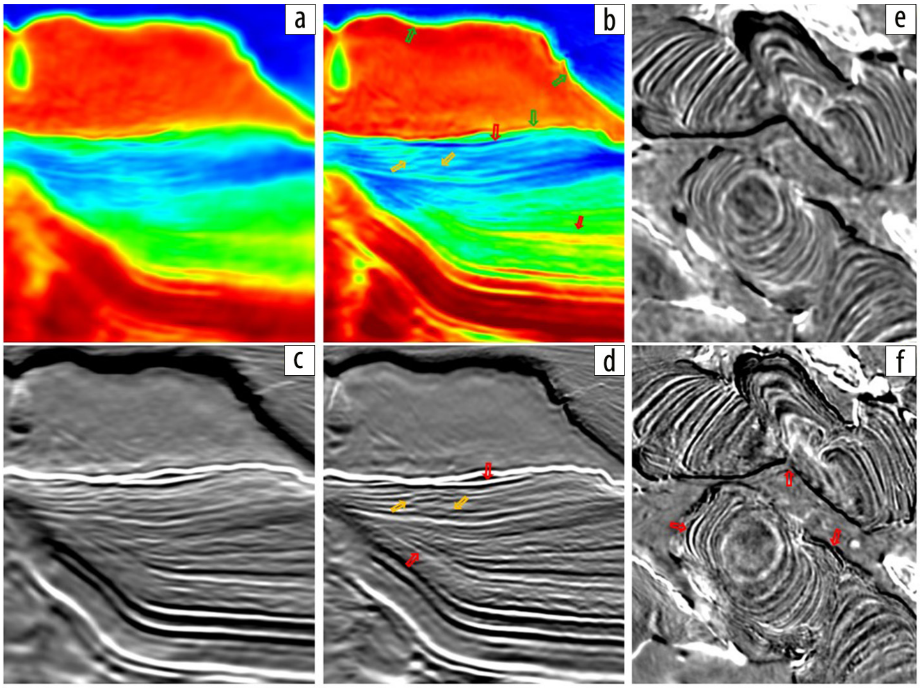

Figure 4. Zoomed part of the velocity model and the corresponding FWI images after acoustic DM FWI in (a) and (c), and elastic DM FWI in (b) and (d), respectively. A depth slice in the FWI images is shown for (e) AFWI and (f) EFWI velocities.

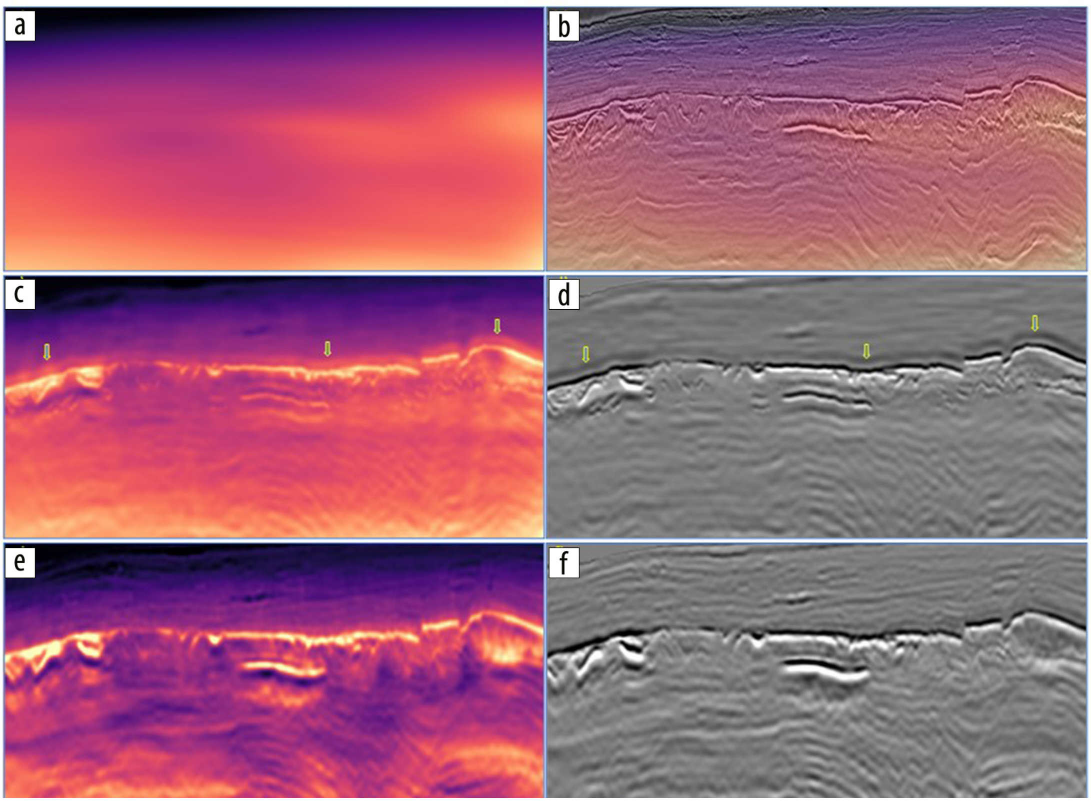

Figure 5. The (a) legacy model and (b) the Kirchhoff migration image with it. (c) Acoustic DM FWI model. (d) FWI image. (e) EFWI velocity model and (f) the corresponding FWI image.

Narrow-azimuth data from the Nile Delta

The Nile Delta area has high hydrocarbon potential, particularly for gas exploration. However, the complex geology poses significant challenges for seismic imaging. The post-Messinian section contains mud volcanoes and small gas pockets, leading to strong lateral variation in rock properties that complicate the imaging. The Messinian layer itself, consisting of a mix of sands, shales, and evaporites, is rather complex due to its disruption by faults and mobile shale. This complexity is further compounded in the pre-Messinian section, where the overlying geologic features create difficulties in accurate velocity model building and imaging (Davies et al., 2024). To address these challenges, advanced seismic processing methods, including high-resolution velocity model building and cutting-edge imaging algorithms, are essential.

Starting with the legacy model shown in Figure 5a, both acoustic and elastic DM FWI are applied to the raw hydrophone data from a narrow-azimuth streamer survey with limited preprocessing applied. Figures 5c–5f present a comparison of the derived velocity models using acoustic and elastic DM FWI (Figures 5c and 5e), and the corresponding FWI images are shown (Figures 5d and 5f). While acoustic DM FWI results in a relatively high-resolution model, it introduces a pronounced smearing at the top of the Messinian layer (indicated by yellow arrows in Figure 5c), resulting in a false low-frequency horizon in the FWI image (Figure 5d) that may cause potential interpretation errors. The elastic DM FWI velocity enhances the resolution in comparison to the acoustic result and reduces the smearing effect. Elastic DM FWI effectively captures the top contrasts as well as small-scale features within the Messinian layer, providing better resolution of this complex layer. Figures 6a and 6c show depth slices through the post-Messinian layer for the two final FWI velocity models. Figures 6b and 6d are respectively the corresponding FWI images. The EFWI model more clearly defines the two mud volcanoes with higher resolution (bottom left in Figure 6c), as well as improves the imaging of the channels (top right in Figure 6d). Additionally, elastic DM FWI captures small gas pockets, as shown by the arrows, which are not visible in the AFWI model.

The model building flow is finalized by applying FWI for a maximum frequency of 20 Hz following the 10 Hz elastic DM FWI result. This final velocity model adds further detail for the post-Messinian section such as mud volcanoes, channels, and small gas pockets (Figure 6e). Kirchhoff migration with the final velocity model is shown in Figure 7b overlaying the velocity model. Comparing with the image from the legacy model shown in Figure 5b, Figure 7c shows, as pointed to by the arrows, much more geologically plausible structures in the pre-Messinian zone with better focused faults. The final velocity model also produces a highly detailed FWI image (Figure 7d) with better illumination and much improved resolution comparing to the Kirchhoff migration result shown in Figure 7c.

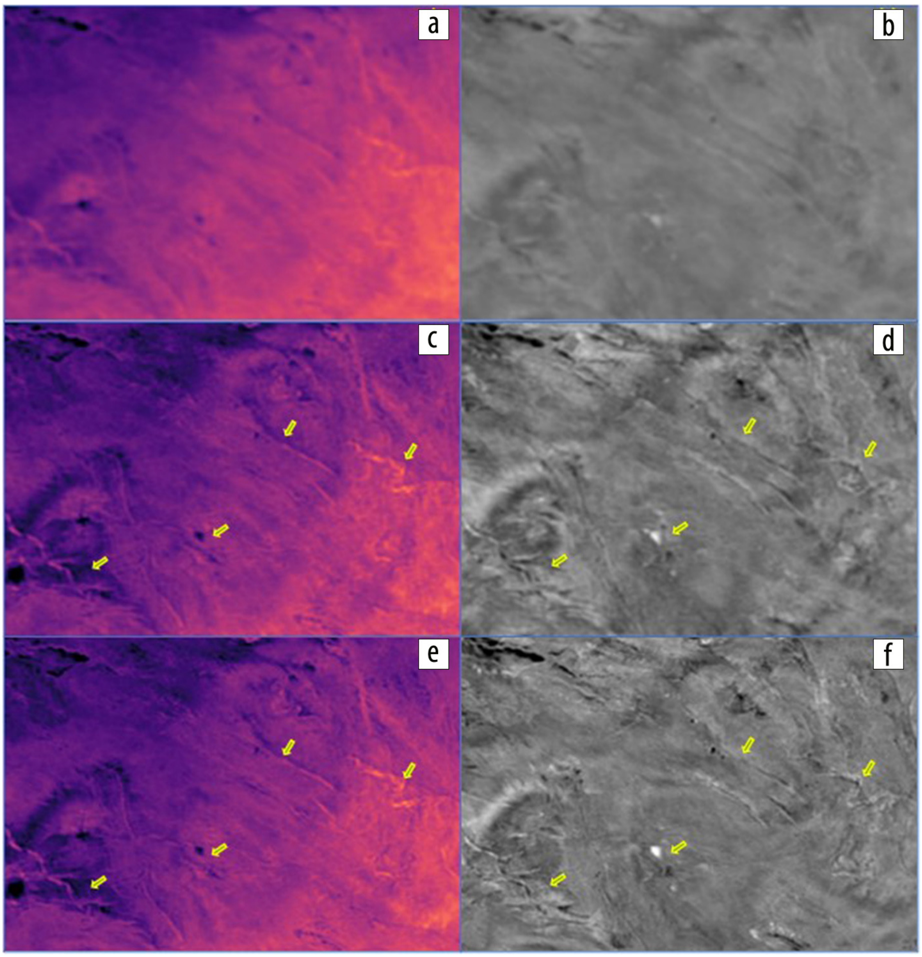

Figure 6. Post-Messinian velocity model depth slice: (a) acoustic DM FWI, (c) elastic DM FWI, and (e) the final model. (b), (d), and (f) Corresponding FWI images.

DAS/VSP example in the GoM

DAS acquisition offers distinct advantages for reservoir monitoring by providing continuous, real-time, high-resolution data from a vast number of sensors along the borehole in a cost-effective manner (Mateeva et al., 2012; Gao et al., 2024). However, the specific VSP-type acquisition geometry brings imaging challenges due to the limited spatial coverage, especially in geologically complex areas like salt or basalt environments, where limited illumination can seriously impact the image quality. Benefited from the more accurate simulation of wavefield using elastic wave propagation and the complementary illumination from mode-converted waves, EFWI can provide a more accurate velocity and a correspondingly better illuminated FWI image.

Figures 8a and 8b show a snapshot of the compressional (P) wavefield generated using acoustic and elastic

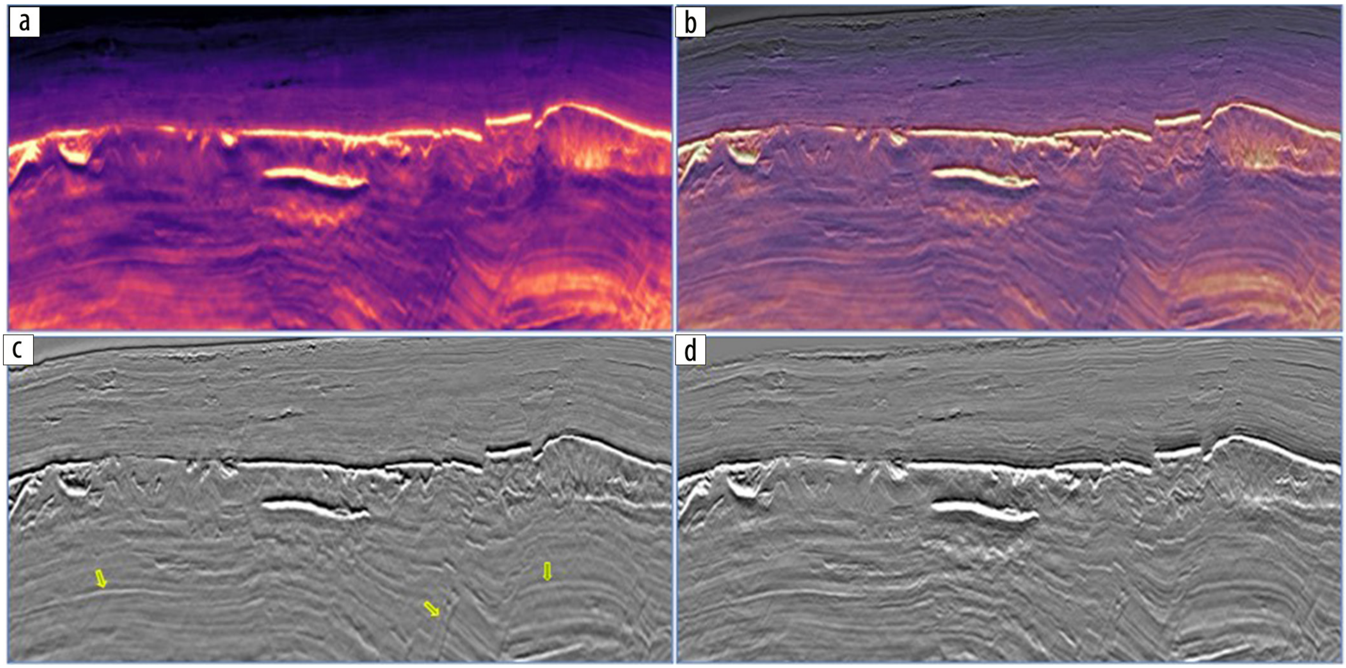

Figure 7. (a) Final FWI velocity model and (b) Kirchhoff migration overlayed with the velocity and (c) without overlaying. (d) FWI image.

wave propagation, respectively, where the red arrow in Figure 8b points to an event in the elastic wavefield that is missing in the acoustic case. This event corresponds to a twice mode conversion at the salt boundary: converted from P to S wave entering the salt body and converted back to P from S wave when exiting the salt body. This conversion is not simulated by the acoustic wavefield. Figure 8c shows a shot gather from the field DAS-VSP data in the GoM, where multiple massive salt bodies are present in the survey area. Figures 8d and 8e show, respectively, the acoustic and elastic synthetic shot gathers. In the numerical simulation, reciprocity was applied with a dipole source being injected to the particle velocity wavefields. As pointed to by the red arrows, elastic wave propagation (Figure 8e) simulates the mode-converted waves presented in the field data (Figure 8c), while such events are missing from the acoustic result shown in Figure 8d.

Starting with a velocity model derived from an OBN survey, both acoustic and elastic DM FWI were applied to the DAS data, and the corresponding FWI images were generated. Figures 9a and 10a show, respectively, one inline and one crossline in the AFWI image volumes, while Figures 9b and 10b are the corresponding inline

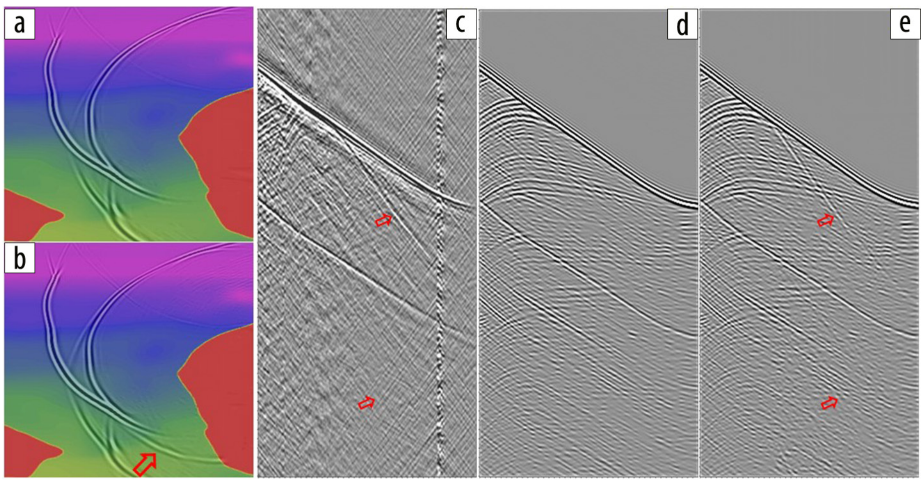

Figure 8. A snapshot of an (a) acoustic and (b) elastic wavefield initiated in the water and propagating through a salt body. The red arrow points to a mode-converted wave. (c) A shot gather from a DAS VSP survey. (d) The acoustically simulated shot gather. (e) The corresponding elastic synthetic gather. The red arrows in (c) and (e) point to mode-converted waves.

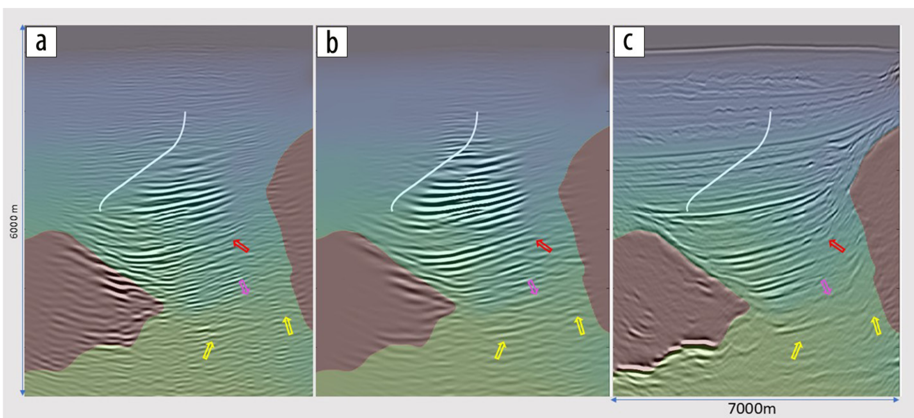

Figure 9. One inline in the FWI image after (a) AFWI and (b) EFWI. (c) The same line in the RTM image of the downgoing component in a conventional OBN survey using the AFWI model. The white line shows the well trajectory of the fiber.

and crossline in the EFWI image volumes. The elastic results show better focusing and more continuous events due to more accurately representing the P-wave energy and taking advantage of the contribution of converted wave signal, as pointed to by the arrows in Figures 9b and 10b, when compared to Figures 9a and 10a, respectively. Properly utilizing these events is particularly important for DAS-VSP data due to the very limited fold coverage associated with this type of acquisition, thus adding to the list of advantages of EFWI over AFWI.

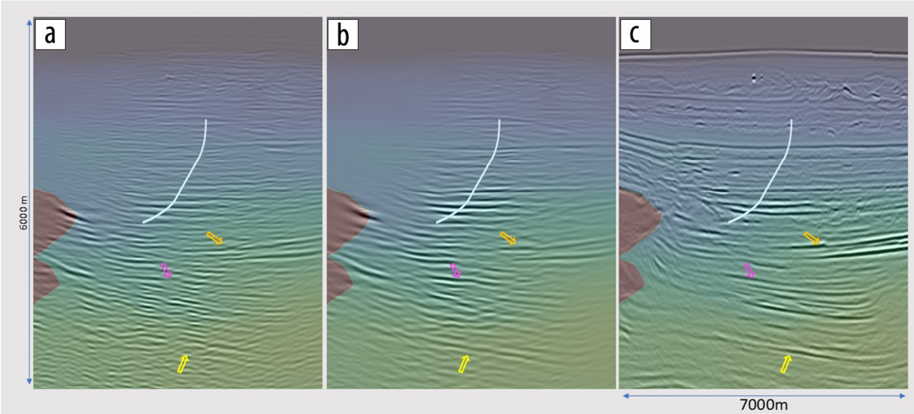

Figure 10. One crossline in the FWI image after (a) AFWI and (b) EFWI. (c) The same line in the RTM image of the downgoing component in a conventional OBN survey using the AFWI model.

As a reference, Figures 9c and 10c show, respectively, the inline and crossline in the RTM image of the OBN data using a velocity model generated by AFWI. In fact, in both lines in the EFWI image shown here, the bottom events indicated by the yellow arrow have better quality than the corresponding events in the OBN RTM image. This improvement may come from the better illumination due to the fact that receivers in a DAS recording are closer to the structures.

Conclusions

In this paper, we demonstrate the advantages of elastic DM FWI. Comparing to AFWI, the employed elastic wave equation can more accurately simulate the wave phenomena, resulting in an improved velocity model with more focused hard interfaces, which better represents the earth's geologic property and thus can significantly improve the imaging of underneath structures. In addition, EFWI can accurately take advantage of the contribution from mode-converted energy at strong interfaces like the salt boundaries that are complementary to the P-wave energy to enhance the illumination of subsalt areas. Though current practices invert V_P only, the inversion makes use of realistic approximations of V_P/V_S and ρ models with well constraints. Applications to different data confirm that EFWI is the preferred algorithm in geologically complex areas. TLE

Acknowledgments

We thank TGS for support and permission to publish this work and our colleague, Olga Brusova, for her help with the well data. We thank TGS Multiclient for the sparse-node data, BP for permission to use the examples from the Nile Delta, and Shell and BP Exploration and Production Inc. for the DAS-VSP data.

Data and materials availability

Data associated with this research are confidential and cannot be released.

Corresponding author: faqi.liu@tgs.com

References

Davies, D., P. Brown, P. Agnisola, V. Valler, M. Romanenko, J. Fruehn, J. Raffle, M. Nicholson, and S. Pan, 2024, Unlocking the Nile Delta subsurface via advanced processing and imaging: The Leading Edge, **43**, no. 9, 596–605, https://doi.org/10.1190/tle43090596.1.

Gao, F., F. Liu, G. Zhan, R. Malik, C. Calderón-Macías, D. Kiyashchenko, and J. Wall, 2024, Maximize the value of DAS VSP using full wavefields: The Leading Edge, **43**, no. 11, 735–739, https://doi.org/10.1190/tle43110735.1.

Huang, Y., J. Mao, H. Xing, and C. Chiang, 2020, Noise strikes, but signal wins in full waveform inversion: 90th Annual International Meeting, SEG, Expanded Abstracts, 805–809, https://doi.org/10.1190/segam2020-3427856.1.

Kumar, D., and R. Ali, 2024, Integration of FWI-derived reflectivity in seismic interpretation: The Leading Edge, **43**, no. 12, 836–842, https://doi.org/10.1190/tle43120836.1.

Liu, F., C. Macesanu, H. Hu, F. Gao, Y. Huang, G. Zhan, J. Sheng, Y. He, C. Calderon, and B. Wang, 2024, Enhance P wave imaging using elastic dynamic matching FWI: 85th Annual Conference and Exhibition, EAGE, Extended Abstracts https://doi.org/10.3997/2214-4609.202410847.

Mao, J., J. Sheng, Y. Huang, F. Hao, and F. Liu, 2020, Multi-channel dynamic matching full-waveform inversion: 90th Annual International Meeting, SEG, Expanded Abstracts, 665–670, https://doi.org/10.1190/segam2020-3427610.1.

Mateeva, A., J. Mestayer, B. Cox, D. Kiyashchenko, P. Wills, J. Lopez, S. Grandi, et al., 2012, Advances in distributed acoustic sensing (DAS) for VSP: 82nd Annual International Meeting, SEG, Expanded Abstracts, https://doi.org/10.1190/segam2012-0739.1.

Plessix, R.-É., and T. Krupovnickas, 2021, Low-frequency, long-offset elastic waveform inversion in the context of velocity model building: The Leading Edge, **40**, no. 5, 342–347, https://doi.org/10.1190/tle40050342.1.

Raknes, E., B. Arntsen, and W. Weibull, 2015, Three-dimensional elastic full waveform inversion using seismic data from the Sleipner area: Geophysical Journal International, **202**, no. 3, 1877–1894, https://doi.org/10.1093/gji/ggv258.

Routh, P., R. Neelamani, R. Lu, S. Lazaratos, H. Braaksma, S. Hughes, R. Saltzer, et al., 2017, Impact of high-resolution FWI in the Western Black Sea: Revealing overburden and reservoir complexity: The Leading Edge, **36**, no. 1, 60–66, https://doi.org/10.1190/tle36010060.1.

Wang, B., Y. He, J. Mao, F. Liu, F. Hao, Y. Huang, M. Perz, and S. Michell, 2021, Inversion-based imaging: From LSRTM to FWI imaging: First Break, **39**, no. 12, 85–93, https://doi.org/10.3997/1365-2397.fb2021096.

Wang, H., O. Burtz, P. Routh, D. Wang, J. Violet, R. Lu, and S. Lazaratos, 2021, Anisotropic 3D elastic full-wavefield inversion to directly estimate elastic properties and its role in interpretation: The Leading Edge, **40**, no. 4, 277–286, https://doi.org/10.1190/tle40040277.1.